ADVANCED ENERGY MATERIALS
www.advenergymat.de

Optical Properties of Organic Semiconductor Blends with Near-Infrared Quantum-Dot Sensitizers for Light Harvesting Applications

Grigorios Itskos, Andreas Othonos, Tobias Rauch, Sandro F. Tedde, Oliver Hayden, Maksym V. Kovalenko, Wolfgang Heiss, and Stelios A. Choulis*

We report an optical investigation of conjugated polymer (P3HT)/fullerene (PCBM) semiconductor blends sensitized by near-infrared absorbing quantum dots (PbS QDs). A systematic series of samples that include pristine, binary and ternary blends of the materials are studied using steady-state absorption, photoluminescence (PL) and ultrafast transient absorption. Measurements show an enhancement of the absorption strength in the near-infrared upon QD incorporation. PL quenching of the polymer and the QD exciton emission is observed and predominantly attributed to intermaterial photoinduced charge transfer processes. Pump-probe experiments show photo-excitations to relax via an initial ultrafast decay while longer-lived photoinduced absorption is attributed to charge transfer exciton formation and found to depend on the relative ratio of QDs to P3HT:PCBM content. PL experiments and transient absorption measurements indicate that interfacial charge transfer processes occur more efficiently at the fullerene/polymer and fullerene/nanocrystal interfaces compared to polymer/nanocrystal interfaces. Thus the inclusion of the fullerene seems to facilitate exciton dissociation in such blends. The study discusses important and rather unexplored aspects of exciton recombination and charge transfer processes in ternary blend composites of organic semiconductors and near-infrared quantum dots for applications in solution-processed photodetectors and solar cells.

1. Introduction

Solution-processed photodetectors and photovoltaics based on organic semiconductor materials represent a promising route to devices that can be processed inexpensively at ambient conditions and can be deposited with printing and coating techniques at large area substrates. A common configuration of such devices is based on binary organic bulk heterojunctions of a conjugated polymer acting as electron donor and a fullerene material acting as electron acceptor. Absorption of light generates excitons that encounter the donor-acceptor heterointerface and dissociate. Exciton dissociation is followed by electron transfer from the polymer to the fullerene that leads to generation of photocurrent. Solar cell devices based on such bulk heterojunctions have recently shown promising results including power conversion efficiencies in the range of 6-7.5%[1,2], lifetime of over 1 year under real environmental conditions[3] and proven proof of concept for high throughput fabrication using printing[4,5] and spray coating technologies[5].

However a significant limitation on the efficiency of such devices is that absorption by the blends is mainly limited to visible wavelengths so that a significant fraction of the solar emission energy, occurring at longer wavelengths, cannot be harvested. To circumvent this limitation, parallel to research for low bandgap polymer materials[6,7] a significant effort has been carried out on the incorporation of red and infrared-absorbing colloidal nanocrystals in bulk heterojunction organic based blends. The main idea, introduced by Alivisatos and coworkers[8] aimed to replace the fullerene component of

Dr. G. Itskos
Department of Physics
Experimental Condensed Matter Physics Laboratory
University of Cyprus
Nicosia, 1678, Cyprus
E-mail: itskos@ucy.ac.cy
Dr. A. Othonos
Department of Physics
Research Center of Ultrafast Science
University of Cyprus
Nicosia, 1678, Cyprus
Dr. T. Rauch, Dr. S. F. Tedde, Dr. O. Hayden
Siemens AG, Corporate Technology
CT T DE HW3, Erlangen, 91058, Germany
Dr. M. V. Kovalenko, Dr. W. Heiss
Institute of Semiconductor and Solid State Physics
University of Linz
Linz, 4040, Austria
Dr. S. A. Choulis
Molecular Electronics and Photonics Research Unit
Department of Mechanical Engineering and Materials Science and Engineering
Cyprus University of Technology
Limassol, 3603, Cyprus

DOI: 10.1002/aenm.201100182

the blends, with an electron acceptor material with controllable absorption properties in the infrared, owing to the presence of quantum confinement effects in the quantum dots (QDs). Significant progress has been made since the first implementation of the idea, with order of magnitude improvement at sensitivity, power conversion efficiency and bandwidth of nanocrystal containing infrared photodetectors and solar cell devices[9–12]. A large number of the efforts reported, employed the QDs to substitute the fullerene component as the electron acceptor material in a conductive polymer-QDs type of heterojunction. However binary and ternary blends combinations, that include fullerene materials, have been also successfully employed[10,11,12]. Most of the early effort has been concentrated on blends that incorporate II-VI QDs mainly based on the Cd(S,Se,Te) system. However there has been growing interest on all-QD or hybrid devices employing IV-VI QDs[9–16](PbS, PbSe, PbTe) owing to their unique properties that include a direct energy bandgap, large dielectric constants, potential for multiple-exciton generation and a large Bohr radius that enables quantum confinement tuning of their band-edge in a wide range spanning from 800 to 3500 nm[17].

Recently efficient hybrid photodiodes based on blends of colloidal, oleic-acid capped PbS QDs, poly(3-hexylthiophene) (P3HT) and methanofullerene derivatives (PCBM) materials with extended spectral sensitivity of up to 1850 nm have been demonstrated[12]. An optimum blend material composite was identified for PbS-QDs absorbing around 1200 nm for which external quantum efficiencies (EQEs) up to 51% at -8 V were observed. The photodiode structures of reference 12 were mainly investigated by contact techniques that probe their overall device performance. However it has been established that the presence of electrodes affects exciton/carrier recombination in the device active layer. To isolate the influence of the electrodes and thoroughly investigate the excitation dynamics in the active layer of such structures we report here a detailed non-contact optical investigation of a systematic unprocessed sample series.

2. Results and Discussion

2.1. Samples

The sample series under study consists of a number of reference pristine and binary blends of the polymer, fullerene and quantum dot materials, along with a series of ternary samples that exhibit a systematic variation of the QDs to P3HT/PCBM relative ratio. To produce the films, materials were dissolved in chlorobenzene under nitrogen atmosphere in a glovebox. Pristine and blend films were deposited in glass substrates by doctor-blade under identical conditions resulting in films of ~150-300 nm. A thermal annealing process was applied subsequently to film deposition (details in experimental section). Blends were fabricated by varying the% weight content on QDs while retaining constant (1:1) the relative weight ratio of P3HT and PCBM. The same QD diameter size was used (~4.4 nm) for all samples, corresponding to the QD size for highest quantum efficiency of the photodetectors of reference 12. The sample compositions being studied in this work along with the corresponding sample thicknesses are summarized in **Table 1**. It can be observed that the incorporation of a larger QD content in the films under identical processing conditions, results in systematically thinner films. **Figure 1** contains a TEM cross-section of a typical ternary sample i.e. 67% QDs along with the three material structures that the blend is composed of. The TEM micrograph dark contrast denotes the presence of the oleic-acid capped PbS QDs, while the light areas correspond to the P3HT and PCBM materials. The image shows that the QDs are uniformly distributed within the P3HT:PCBM matrix. More information on the structural characteristics of the blends can be found on reference 12.

Table 1. Sample compositions and thicknesses with varying content of P3HT, PCBM and PbS QDs.

Sample Abbreviation	P3HT wt%	PCBM wt%	QD wt%	Sample Thickness [±10 nm]
pristine P3HT	100	0	0	300
pristine PCBM	0	100	0	275
pristine QDs	0	0	100	290
P3HT:PCBM	50	50	0	295
P3HT:QDs	33	0	67	185
PCBM:QDs	0	33	67	195
20% QDs	40	40	20	190
40% QDs	30	30	40	265
67% QDs	16.5	16.5	67	165
80% QDs	10	10	80	150

2.2. Absorption

The steady-state optical absorbance of pristine, binary and ternary blend films in the 250-1500 nm range is displayed in **Figure 2**(a), (b) and (c), respectively. In the insets, the magnified absorbance in the red/infrared spectral region (650-1500 nm) is also displayed for clarity. The pristine polymer film (Figure 2(a)) exhibits strong and broad absorption in the 350-650 nm spectral range attributed to ground and excited state π-π^* transitions[18]. Due to the large sample thickness practically all incident light (optical density larger than 3.5) is absorbed in the 450-610 nm

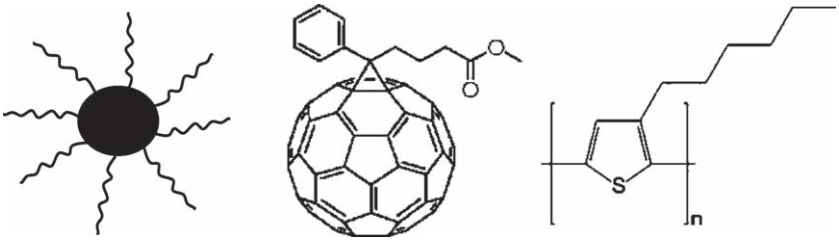

Figure 1. TEM cross-section of the ternary sample 67% QDs. The material structures that the blend is composed of are also displayed.

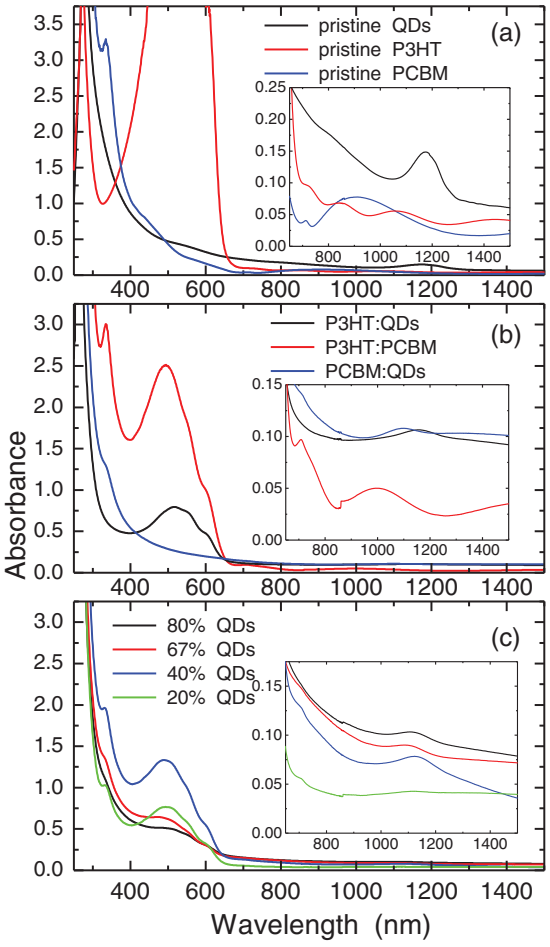

Figure 2. Absorbance of pristine (a), binary (b) and ternary (c) films. In the insets the magnified absorbance in the red/infrared spectral region is displayed for clarity. The contribution to absorption due to the PbS QD ground exciton is clearly observable.

range and the associated P3HT absorption structure cannot be resolved. PCBM exhibits a weaker absorption with a band gap of ~700 nm and PCBM-characteristic high energy features at 335 and 430 nm[19]. Red and near-infrared contribution to absorption due to excitonic interband QD transitions is observable in the inset of Figure 2a, with the feature at 1180 nm identified as the ground state of the PbS QD exciton.

In the binary and ternary films, the absorbance in the visible and red/infrared region is dominated by P3HT and QD transitions, respectively. As expected a scaling of the near-IR absorbance with QD content is observed. However the overall light harvesting strength in the near-infrared range remains rather low i.e. absorption of 10-25% of the incident light. Comparison of the absorbance of the binary P3HT:PCBM and P3HT:QDs blends in Figure 2b shows that the former are blue-shifted by ~25 nm with respect to the latter. Blue-shift of the absorbance of P3HT:PCBM blends relative to that of pure P3HT has been typically attributed[20] to the destruction of the ordering of P3HT chains due to the incorporation of PCBM. On the other hand the absence of a significant spectral shift and the preservation of the P3HT absorption structure in the QD binary sample indicate that the incorporation of even a high QD density does not significantly disrupt the molecular packing of the polymer. In the ternary samples the presence of PCBM results in a similar absorption blue shift to that of the P3HT:PCBM sample, while the polymer absorption structure smoothens for the high QD content (67% and 80%) samples. This indicates that the simultaneous presence of PCBM and a high QD content affects the crystallinity of P3HT. The implications of the polymer-fullerene mixing in the device performance have been recently highlighted in a publication[21] using X-ray spectroscopy; a similar structural study could shed further light on the nature of the ternary blend interpenetrating nanostructure. Another characteristic of Figure 2b is the observation of the significant reduction in the absorbance strength (~ factor of 3) in the spectral region of the P3HT absorption in the binary sample P3HT:QDs relative to that of the P3HT:PCBM system. The reduction is attributed to the smaller thickness and the reduced polymer content (33 wt%) in the former sample relative to the latter (50 wt%). Other factors such as light scattering due to the large contrast between the index of refraction of PbS (n ~ 4) and that of the P3HT:PCBM matrix (n ~ 1.8[22]) are also expected to influence the absorption of QD-containing samples.

2.3. Photoluminescence

Comparative photoluminescence spectra (PL) from the samples in the spectral region of the P3HT and QD emission are shown in **Figure 3**a and b respectively. No study of the PCBM emission was performed as it was too weak to be detected even from the pristine fullerene sample. The P3HT emission contains characteristic vibronic peaks at ~660 and ~720 nm while the sharp feature at ~810 nm is due to the second-order diffraction of the excitation source (λ = 405 nm) by the spectrometer grating used. No significant modification of the structure and wavelength position of the polymer emission was observed within the samples. Emission from the QDs is dominated by a broad featureless peak attributed to the QD ground state exciton. The PL peaks exhibit Stokes shifts in the range of 50-60 nm (43-53 meV) from the corresponding absorption features while the wavelength position of the peaks vary in the 1165-1240 nm region. Interestingly an almost systematic blue-shift of the peaks (up to ~75 nm) can be observed as the PCBM relative content of the samples is increased. The shift is also visible in the absorption spectra (insets of Figure 2b and Figure 2c) and could be attributed to slightly different QD size distributions in the samples; however owing to its systematic dependence with PCBM content it could also be due to structural reorganization of the blends upon PCBM addition or due to intermaterial electronic interactions i.e. based on the approximate materials band offsets[12] the shift could indicate the formation of a charge-separated bound state in which the electron resides in the PCBM while the hole remains in the QDs. Such a hypothesis will be addressed by time-resolved experiments in the QD region and will be the topic of future work.

The main observation however from Figure 3 is that the PL intensity in the blend samples is quenched relative to that of

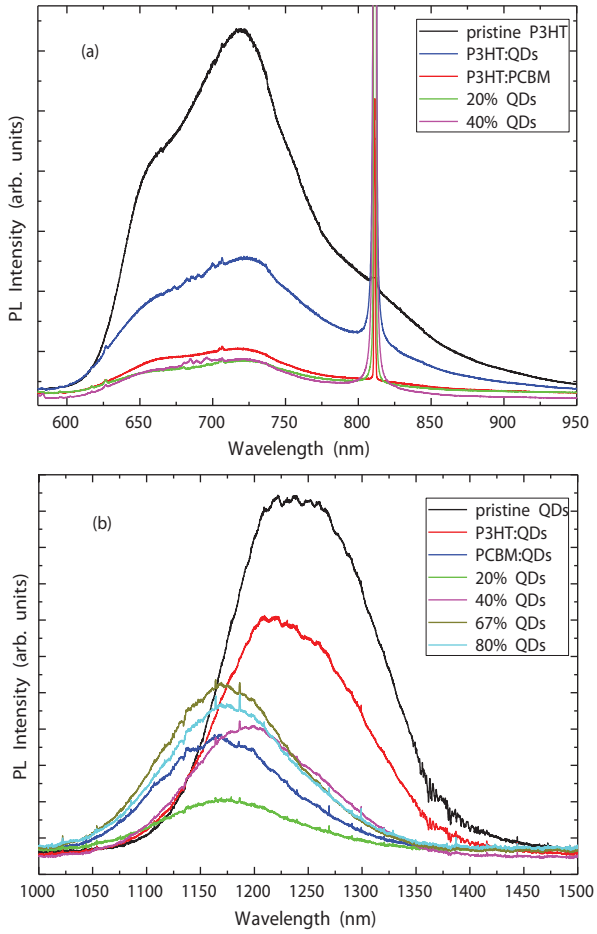

Figure 3. Photoluminescence spectra from pristine, binary and ternary samples in the spectral regions of the P3HT (a) and QD exciton (b). The blend emission is partial quenched with larger quenching ratios observed in the P3HT region. The inclusion of the fullerene in the blends seems to promote exciton dissociation.

the pristine samples, in both the P3HT and the QDs emission region. The PL quenching ratio is quantified by the equation:

$$PLquenchingratio = \frac{I_{pristine} - I_{blend}}{I_{pristine}} 100\% \quad (1)$$

Where $I_{pristine}$ and I_{blend} are the integrated PL intensity from the pristine and blend samples, respectively measured in the emission region of the P3HT or the QDs. To take into account the variations in the sample composition and thickness, the laser excitation density was normalized to the optical absorbance (optical density) of each sample at the excitation wavelength used i.e. the laser power was adjusted to approximately photogenerate an equal density of carriers/excitons at all samples. **Table 2** contains the summary of the PL quenching ratios obtained from the comparative study. The errors represent the standard deviation of the quenching ratios across the sample surface to account for thickness and composition variations (details in experimental section).

PL quenching can probe the fraction of photoexcited excitons that are fluorescent. Such exciton fraction is small (~1%[23]) in P3HT, while it is significantly larger in the PbS QDs (~20%[39]). PL experiments are thus more representative of the total number of photoexcited excitons in the QDs rather than in the polymer emission region. Nevertheless even in the latter region PL experiments can provide some indirect information on the P3HT exciton dissociation process. The approximate energy band offsets of the blend materials[12] are displayed in **Figure 4**. In the same diagram, the following energetically allowed interfacial charge transfer processes that could result in emission quenching of P3HT (processes 1,2, blue dotted lines) and QDs (processes 3,4, red dotted lines) in the blends are depicted: (1) electron transfer from P3HT to PCBM, (2) electron transfer from P3HT to QDs, (3) electron transfer from QDs to PCBM and (4) hole transfer from QDs to P3HT.

Table 2. Summary of PL quenching experiments.

Sample	PL Quenching Ratios P3HT region	PL Quenching Ratios QD region
P3HT	0	-
QDs	-	0
P3HT:PCBM	85.2±7.9%	-
P3HT:QDs	55.4±13.2%	34.6±11.5%
PCBM:QDs	-	65.4± 9.1%
20% QDs	87.3±17.3%	80.2± 18.9%
40% QDs	89±12.8%	65.3± 11.9%
67% QDs	Traces of PL	52.7± 9.8%
80% QDs	Traces of PL	55.8± 12.5%

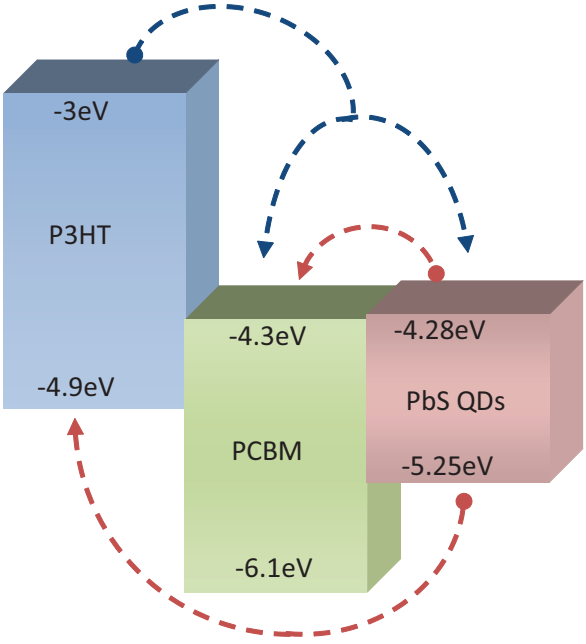

Figure 4. Diagram of the energy band offsets of the blend materials. Interfacial carrier transfer channels potentially responsible for the emission quenching of P3HT (blue dotted lines) and QD (red dotted lines) are also depicted.

We first discuss emission quenching in the polymer region. There is a general consensus in the literature that ultrafast photoinduced electron transfer from P3HT to PCBM is responsible for the efficient quenching of the polymer emission in P3HT:PCBM films. The P3HT emission quenching mechanism in QD-containing blends may additionally involve processes mediated by the QDs such as electron transfer to QDs, radiative pumping i.e. re-absorption of the polymer fluorescence by the QDs and/or non-radiative energy transfer to the QDs. Quenching of P3HT emission due to re-absorption by the QDs has been proposed as the main quenching mechanism in a number of studies of PbS QDs in conductive polymers[24,25]. In general, efficient quenching of the polymer emission can occur via either radiative and/or non-radiative intermaterial coupling. In fact if a fast resonant energy transfer process to the QDs i.e. faster than the other P3HT exciton dissociation mechanisms is present in our samples it can potentially result, in addition to polymer emission quenching, to QD emission enhancement. Signatures of such emission redistribution were not observed from any sample involved in this study. To further investigate the issue we have performed a PL study of the P3HT:QDs sample with a high power (140 mW) light emitting diode, emitting at 505 nm, while detecting the emission at both the P3HT and QD PL region. At such wavelengths, absorption by P3HT exceeds by orders of magnitude the absorption of the two other blend components (Figure 2a) so that virtually all excitations are photogenerated in the P3HT. The resulted PL spectrum (not shown) was dominated by the P3HT emission, containing very weak emission from the QDs indicating the absence of significant resonant electronic transfer from the exciton polymer states into the core QD states. It is likely that the dipole-dipole coupling is inhibited among other possible causes, by the rather weak spectral overlap of the P3HT emission and the QD absorption and the dielectric screening of the Coulombic interaction between the polymer and QD excitation dipoles. Investigation of the emission quenching mechanisms in the spectral region of the QD exciton is simpler as no significant spectral overlap of the QD emission with the absorption of P3HT and/or PCBM exists owing to the QD low energy band-edge, so that radiative pumping and Förster energy transfer originating in the QDs cannot occur. Thus the most probable quenching mechanisms appear to be interfacial electron transfer to PCBM and/or hole transfer to P3HT.

It is evident that the presence of all the aforementioned processes complicates the interpretation of the PL quenching data. However some observations can be made owing to the investigation of a systematic series of binary and ternary samples and the implementation of statistics, summarized in Table 2. The data from the binary samples in the second column indicate that quenching of the P3HT emission due to electron transfer to PCBM is more efficient than the corresponding processes mediated by the nanocrystals i.e. electron transfer to QDs and/or re-absorption of the P3HT emission by the QDs. P3HT emission quenching tends to increase with increasing QD content (decreasing P3HT/PCBM content) in the ternary samples which seems to contradict the results of the binary samples i.e. that quenching of the P3HT emission due to PCBM is more efficient than quenching processes due to QDs. However the further reduction in the PL signal could be attributed to other factors such as enhanced Fresnel surface reflection owing to the large contrast between the index of refraction of the PbS QDs and air as well as due to the inefficiency of the correction performed in the PL data at low polymer content. The results of Table 2 also indicate that quenching of the QDs emission due to electron transfer to PCBM is more efficient than quenching due to hole transfer to P3HT. Photodiodes with near-infrared EQE values of 2.3 and 0.2% have been fabricated[12] by binary PCBM:QDs and P3HT:QDs blends, respectively with active region layers similar to the binary films studied here. The considerable larger EQE values of the former devices are supportive of the PL quenching experiments i.e. the presence of more efficient interfacial charge transfer processes in the PCBM:QDs system relative to that of P3HT:QDs. Recent studies[26] are also supportive of the presence of efficient electron transfer from oleic acid-capped PbS QDs to PCBM. Overall larger quenching ratios are observed in the P3HT emission region than in the QD region on the spectra of the same sample which is indicative of a reduced efficiency of the charge transfer processes originating in the QDs. The results are in general agreement with other studies of blends employing oleic acid capped QDs that report inhibition of the charge transfer process by the insulating QD capping layers or by the presence of phase separation due to aggregation of the nanocrystals[27].

Further information on the nature and the quenching mechanism of the fluorescent excitons in the QDs can be obtained from excitation-dependent PL experiments. The summary of the measurements, normalized at the lowest excitation density is presented in **Figure 5** and shows a systematic variation on the PL excitation dependence in the samples. Least-square fits of the corresponding log-log plots (shown in the inset for the bare QDs and the two binary blends) reveal a shift from a sublinear dependence in the pristine QDs sample (gradient ~0.71) and the binary P3HT:QDs sample (gradient ~0.81) to a linear relationship in the binary PCBM:QDs sample. The integrated emission from the ternary samples shows a sublinear depend-

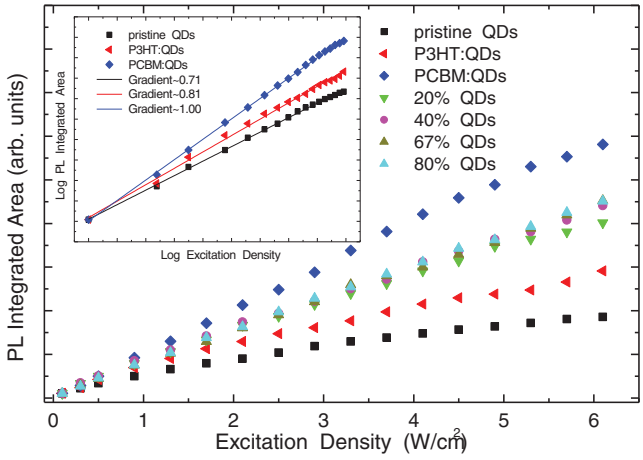

Figure 5. PL integrated intensity versus excitation density in the spectral region of the QD exciton. The inset contain the associated log-log plots from the pristine QDs and the binary P3HT:QDs and PCBM:QDs samples and the corresponding least square fits (red lines). A transition from radiative to non-radiative exciton recombination is observed as samples with lower PL quenching ratios are probed.

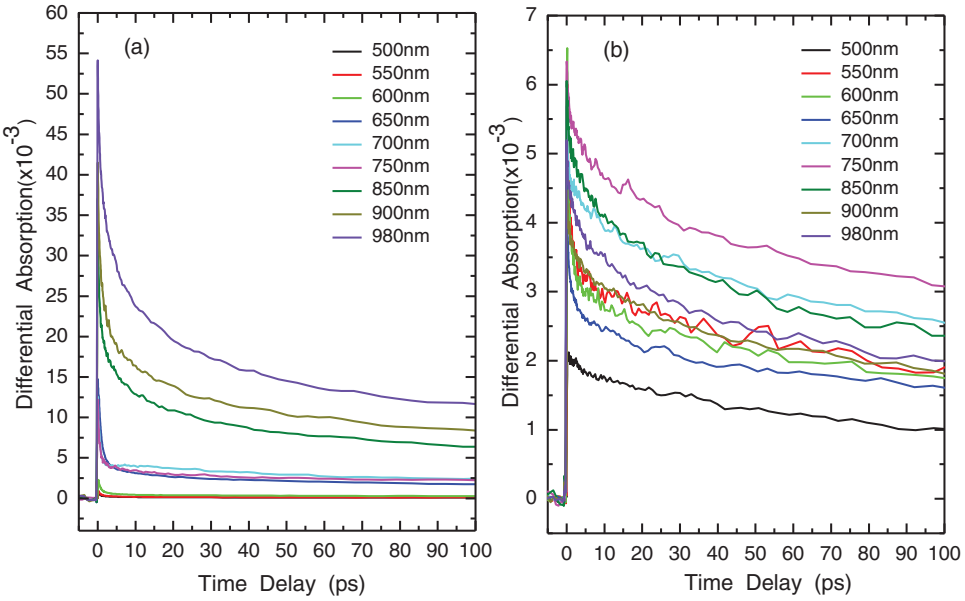

Figure 6. Transient pump-probe absorption of (a) pristine P3HT film, (b) pristine PCBM film. Ultrafast decay constants are attributed to vibronic relaxation of hot excitons while longer constants are due to non-radiative exciton recombination. Quenching of the signal due to partial filling of the P3HT exciton states is observed for short wavelengths probes (6a).

ence on excitation density with gradient values (0.87-0.92) in-between those of the two binary samples. A linear variation of the integrated QD emission with excitation density suggests that the luminescence is dominated by monomolecular recombination due to free excitons. On the other hand the sublinear behavior observed is indicative of the presence of non-linear exciton effects. At the pump fluencies used in our study, it has been found that Auger recombination is the dominant recombination mechanism in PbS QDs[28] if more than one exciton is excited per dot. It can be observed (Table 2) that samples showing large PL quenching ratios or equivalently weak emission i.e. the PCBM:QDs sample, exhibit an excitation-dependence closer to linear than samples with strong emission i.e. bare QDs or the P3HT:QDs sample. In the former samples, it seems that within the pump fluencies studied, exciton dissociation is efficient enough to maintain on the average, one exciton per dot that recombines radiatively. Indeed electron transfer times of 130-150 ps from similar oleic-acid PbS QDs to PCBM have been reported[29] which compete favorably to measured Auger times[28,29]. It is possible that the reduced efficiency of the interfacial charge transfer process in the other blends, allows multiple excitons per dot, thus promoting Auger recombination against radiative recombination.

2.4. Transient Pump-Probe Absorption

To investigate the dynamical evolution of photogenerated excitations in our samples we have employed ultrafast optical pump-probe absorption measurements. Such measurements allow studies of high time-resolution at a subpicosecond range and the possibility of probing both excitonic (fluorescent and non-fluorescent excitons) and unbound carrier relaxation in our samples[23]. The measurements were carried out using a pump wavelength at 400 nm and probe pulses at nine wavelengths in the 500-980 nm spectral range. The spectral resolution of our system did not allow probing at infrared wavelengths larger than 980 nm, so that direct probing of the QD exciton ground state in the blends could not be performed. At a pump of 400 nm all the materials of the blends were photoexcited with the great majority of the excitations however being generated at the P3HT due to its significantly higher absorption at this wavelength (see Figure 1a). **Figure 6** contains the transient absorption measurements of the P3HT and PCBM pristine films. The P3HT transients are described by multi-exponential decays denoting the presence of various excitations relaxation mechanisms. For the purpose of the following discussion a triple exponential rate model was found to provide an adequate fitting of the transient decays (bi-exponential fits fail to adequately describe the decays at short pump-probe delays):

$$I(t) = A_1 e^{-\frac{t}{t_1}} + A_2 e^{-\frac{t}{t_2}} + A_3 e^{-\frac{t}{t_3}} \quad (2)$$

All decays can be modeled by an ultrafast component with sub-picosecond time constant t_1 in the range of 0.4-0.8 ps, a fast component with time constant t_2 in the 5-10 ps range and a considerable longer decay t_3 in the 150-250 ps range. **Table 3** contains the amplitudes and time constants of the transient decays obtained by lineshape analysis with the aforementioned model.

The behavior of the P3HT absorption transients based on both the observed transient amplitude and the contribution of the three decay terms can be roughly divided into three wavelength probe regions. For probes in the 850-980 nm region, large positive signals denoting the presence of strong photoinduced absorption to higher exciton or carrier P3HT states, can be observed. At this region, the contribution of the ultrashort

Table 3. Summary of P3HT transient decay linefitting analysis. $A_{1,2,3}$ and $t_{1,2,3}$ denote respectively the amplitude and time decay fitting values obtained using model (2).

Probe Wavelength (nm)	A_1 [x 10^{-3}]	t_1 [ps]	A_2 [x 10^{-3}]	t_2 [ps]	A_3 [x 10^{-3}]	t_3 [ps]
500	1.7	0.6	0.5	5	0.4	244
550	0.9	0.6	0.2	5.3	0.2	229
600	2	0.6	0.5	4.9	0.4	240
650	12.4	0.7	1.6	7.4	2.7	227
700	11	0.4	2.2	7.1	3.7	245
750	7.2	0.5	2.8	8.4	4.5	237
850	15.6	0.5	10.2	6.1	11.9	160
900	15.3	0.7	11	7.2	14.8	182
980	14.8	0.8	17.3	8.8	20	198

subpicosecond component is approximately equal to that of the long-lived relaxation mechanism. A second probe wavelength region in the 650-750 nm range, spectrally coincident with the P3HT fluorescence, contains decays with smaller transient amplitudes and a larger relative contribution from the short decay terms. At the third probing region for wavelengths shorter than 650 nm, differential absorption signals weaken further and almost diminish. The region coincides with the P3HT ground state exciton states and the quenching of the differential absorption is attributed to partial filling of the probed states. The weak photo-induced absorption observed is dominated by the subpicosecond-lived component in this probe region.

At the pumping wavelength of 400 nm used, higher-energy P3HT singlet excitons are photo-excited that relax to the ground state exciton states at ultrafast rates. The assumption here is that the pump pulse photogenerates predominantly excitons. This is in general agreement with the literature despite the fact that a minority photoexcitation species of free charges seems to also be present in P3HT films[23]. Previous experimental reports on ultrafast spectroscopy on P3HT[30,31] attribute the initial ultrafast relaxation decay to non-linear exciton-exciton annihilation processes that have been found to dominate the ultrafast response of transient absorption signals even at moderate pump fluencies, such as those we used to excite the films (50 μJ/cm^2). To investigate such a hypothesis in our samples, an excitation dependent pump-probe study of the pristine P3HT film was carried out. The measurements were carried out at 4 different excitation densities i.e. 10, 25, 50 and 100 μJ/cm^2 using the same pump and probe wavelengths used in the study of Figure 6. The normalized results for the probe wavelengths of 650 nm and 980 nm are displayed in Figs. 7a and 7b, respectively. Both decays show similar kinetics at the 3 higher excitation densities used. At the lowest fluence of 10 μJ/cm^2 the contribution of the faster decay terms is moderately reduced, with the effect being more pronounced at the probing wavelength of 650 nm. Similar kinetics were observed in the transients at other probe wavelengths. The absence of significant variation of the decay kinetics with excitation density indicates that second-order effects may be present but are not the primary relaxation channel of excitations at the laser fluencies used. This is

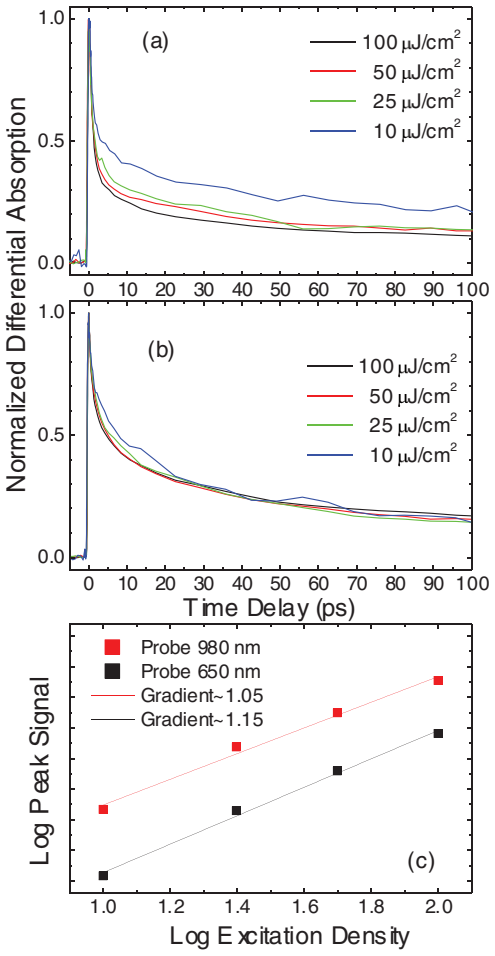

Figure 7. Normalized differential absorption versus laser excitation density at probe wavelengths of (a) 650 nm and (b) 980 nm. (c) Log-Log plots of the pump probe peak signal versus excitation density for the aforementioned probe wavelengths. The small variation of the decay kinetics with excitation density is indicative of first order exciton relaxation (7a and b). This is further supported by the approximately linear dependence of the transient peak signal with excitation density (7c).

further supported by the fact that the transient absorption peak signal at all probe wavelengths, exhibits an approximately linear dependence with excitation density. This is shown in **Figure 7**c, where least-square fits of the log-log plots of the pump-probe peak signals with the excitation densities at probe wavelengths of 650 and 980 nm, reveal gradient values close to 1. We thus conclude that the decay kinetics are dominated by linear effects due to monomolecular recombination most likely attributed to excitons. We hypothesize that the two ultrafast decay terms are due to fast vibronic relaxation of hot excitons photoexcited at higher lying exciton states with the 400 nm pump pulse, while the longer decay is due to non-radiative recombination of P3HT singlet excitons, reported lifetimes (~200 ps) of which[22] seem to coincide with the decay constants observed in our data.

In the PCBM film, transients in Figure 6(b) can be approximated with bi-exponential decays with a short time constant in the 2-5 ps range and a longer time constant in the range of 160-190 ps. The transient signals are an order of magnitude

smaller than those in P3HT, resulting in decays with lower signal to noise ratio. Unlike the P3HT transients, no systematic variation of the transients with probe wavelengths is observed and the contribution of the longer decay is found more significant at all probe wavelengths. Similarly to the interpretation of the P3HT measurements, the fast decays are attributed to hot exciton relaxation processes while the longer decay is attributed to non-radiative singlet exciton relaxation. A pump-probe study of PCBM performed at similar excitation fluencies to ours[32] attributes the initial rapid decay predominantly to exciton-exciton annihilation effects. However the study employs a 330 nm pump, where PCBM absorbs orders of magnitude stronger than the 400 nm pump used in our experiments (see Figure 2a); the significant larger population of photoexcitations created in the former case justifies the appearance of second-order effects.

Following the discussion on the measurements of pristine films, we analyze the pump-probe experiments of the blend samples. To illustrate the variations in the decays compared to pristine films and within the different blends, normalized pump-probe transients are plotted in comparative graphs. Initially the results of the longer wavelength probing region of 650-980 nm are discussed. The transients in this region from all samples are dominated by large positive signals due to photoinduced absorption. **Figure 8** (a–d) contain the normalized decays from the P3HT-containing samples. Representative line-shape fitting parameters obtained using the rate-model (2) at the probe wavelength of 650 nm, are included in **Table 4**.

The decays exhibit interesting patterns defined by material content and probe wavelength. The binary P3HT:PCBM along with the low-QD content ternary samples of 20% QDs and 40% QDs exhibit almost identical decays at all probe wavelengths which indicates that the transient absorption is predominantly defined by the polymer/fullerene components. Similar to the pristine P3HT film, the decays of such samples are characterized by two fast decay components and a slower decay term. However in this case the long-lived component is considerable longer (700-900 ps) compared to that of the pristine polymer films, while its amplitude is larger than that of the ultrafast components, in particular at probe wavelengths of 750 and 850 nm, at which it dominates the signal decay. The component is attributed to the recombination of long-lived charge-transfer excitons that are formed subsequent to carrier transfer at the P3HT:PCBM interfaces of the blends.[33] Charge transfer excitons represent the intermediate step between exciton dissociation and free polaron generation in bulk heterojunction solar cell structures. There has been a mounting recent evidence of their long-lived presence at the donor:acceptor heterointerfaces with reported lifetimes lying in the 1–100 nanosecond regime for polymer–fullerene systems.[33] Our assignment agrees with the results of terahertz photoconductivity studies[34] that probed exciton decay of P3HT:PCBM films at the same spectral region (800 nm) and found the photoconductivity signal to be dominated by charge-transfer excitons at similar timescales to those we have observed (up to 1 ns).

The decays of the pristine P3HT film and the binary P3HT:QDs sample exhibit a different behavior compared to the aforementioned samples. At all probe wavelengths (650-980 nm) the decays of the samples are dominated by the subpicosecond

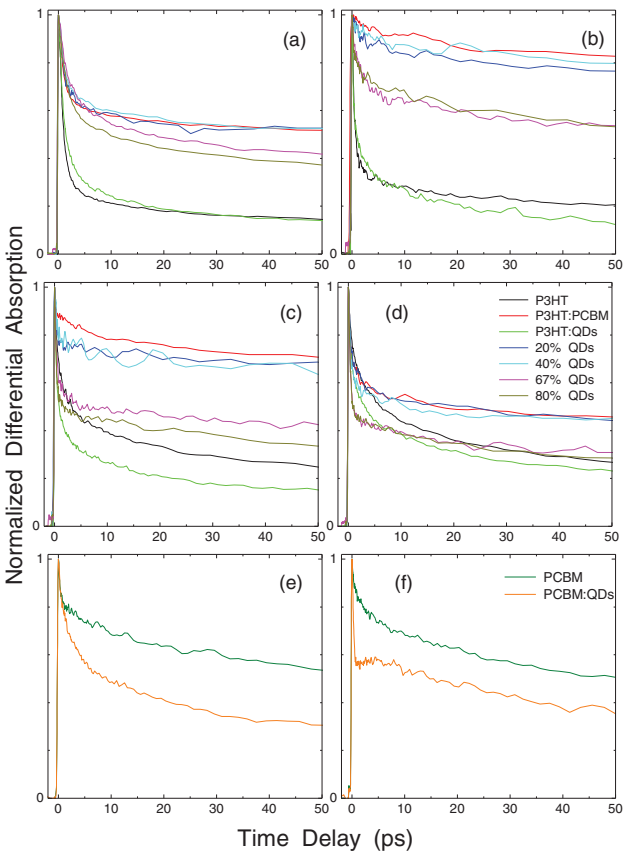

Figure 8. Normalized differential absorption from P3HT-containing samples at probe wavelengths of 650 nm (a), 750 nm (b) and 850 nm (c) and 980 nm (d). Normalized transients from the PCBM film and the PCBM:QDs blend are plotted for probes of 650 nm (e) and 900 nm (f). Long lived decays observed mainly in the P3HT:PCBM and the low-QD content ternaries are attributed to charge transfer exciton recombination.

exciton effects, with a smaller contribution from a longer-lived component (100-250 ps), which we previously assigned to non-fluorescent P3HT excitons. At the shorter probe wavelength (650 nm) a slightly larger contribution of the fast decay is observed in the neat polymer sample compared to that of the QD-containing film, however the situation reverses and progressively

Table 4. Parameters of the normalized transient decay linefitting analysis at probe wavelength of 650 nm.

Sample	A_1	t_1 [ps]	A_2	t_2 [ps]	A_3	t_3 [ps]
P3HT	0.88	0.6	0.13	8.2	0.18	220
P3HT:QDs	0.79	0.9	0.11	10.3	0.16	252
P3HT:PCBM	0.44	0.6	0.16	6.8	0.54	903
20% QDs	0.45	0.6	0.17	6.8	0.53	908
40% QDs	0.33	0.9	0.15	10.4	0.54	898
67% QDs	0.29	1.1	0.23	11	0.46	719
80% QDs	0.33	1.3	0.2	13.3	0.4	818

the ultrafast contribution becomes significant larger in the binary film as longer probe wavelengths are employed. The effect could be due to the additional contribution of a fast exciton relaxation mediated by the QD states i.e. a fast exciton dissociation process at the polymer/nanocrystal interfaces. Ternary samples with a relatively high QD content (67% and 80%) and a concomitant low polymer/fullerene content, exhibit transient signals with characteristics in shape and kinetics intermediate to the two other groups of samples discussed. In particular, their behavior resembles that of the P3HT:PCBM and the low QD-content ternary samples at a probe wavelength of 650 nm, where decay due to the long-lived component attributed to charge exciton formation is dominant. Progressively the ultrafast decay becomes more significant as longer probe wavelengths are employed, with the decays resembling closer the decays of the binary P3HT:QDs sample.

Figure 8 (e) and (f) contain normalized transients for the PCBM pristine film and the binary PCBM:QDs sample. The displayed transients of the binary sample are representative of the shape of the pump-probe signal of the two samples across the 650-850 nm and 900-980 nm probing region, respectively. At the first region, compared to the decays of the neat PCBM film the binary sample shows a larger contribution of the fast relaxation component. In the second region, a sharp subpicosecond component dominates the transient decay, followed by a long-lived decay similar to that of the bare PCBM film. The first region coincides energetically with states of the PCBM ground exciton. The faster decay of the transient signal in the PCBM:QDs sample could possibly be due to PCBM singlet exciton dissociation at the fullerene/nanocrystals interfaces.

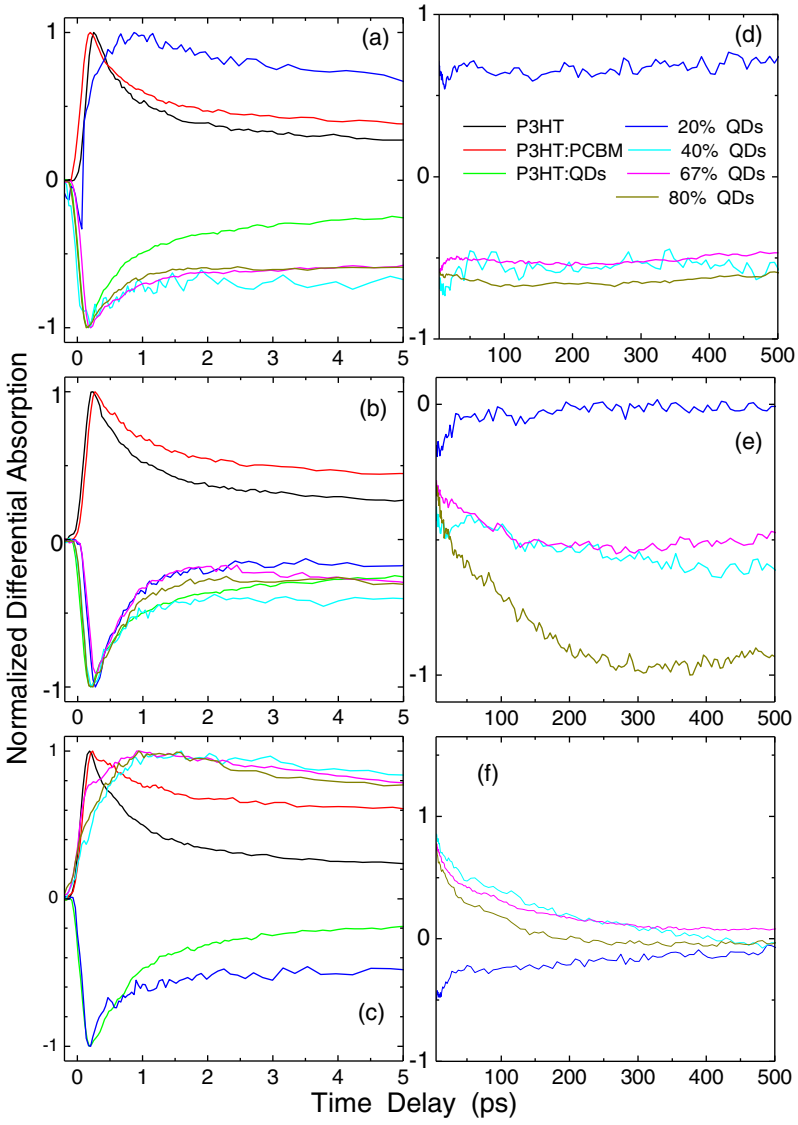

Figure 9. Normalized differential absorption from P3HT-containing samples at probe wavelengths of 500 nm (a), 550 nm (b) and 600 nm (c) for short pump-probe delay times. Normalized transients from ternary blends at long pump-probe delay times are plotted at the same probe wavelengths i.e. 500 nm (d), 550 nm (e) and 600 nm (f). Samples containing both QDs and P3HT exhibit a clear photobleaching. The QD-containing samples exhibit visibly slower signal rise times compared to non-QD containing films.

The normalized differential absorption from the P3HT-containing samples is plotted for short-wavelengths probes (500-600 nm) in **Figure 9**. The region probed coincides with the P3HT singlet exciton ground states. Figure 9(a), (b) and (c) contain data at short pump-probe delay times while Figure 9(d), (e) and (f) contain the ternary samples transients at long pump-probe delay times (5-500 ps) across the same probe wavelengths. A general observation is the appearance of negative transient signals in the decays of some of the blend samples compared to small but positive signals observed across the same region in the pristine P3HT film. The negative signals denote the presence of absorption photobleaching due to filling of the polymer exciton states in the blends. Inspection of the transient signals shows that only samples containing both QDs and P3HT exhibit a clear photobleaching in all or some of the three probing wavelengths (500-600 nm). Furthermore a general trend of increase of the photobleaching amplitude with increasing QD concentration can be observed in the non-normalized decays of the ternary samples (not shown). We infer then that the bleaching comes as a result of exciton and/or carrier dynamical processes between the P3HT and the QDs that result in the filling of the exciton states of the former. In the case of samples containing P3HT but no QDs i.e. the bare polymer and the P3HT:PCBM blend, the absence of complete photobleaching i.e. negative pump-probe signal, across the same probing region is attributed to the considerably larger P3HT fluorophore density of the former compared to that of the blends and to the efficient P3HT exciton dissociation occurring in the latter that depletes efficiently the P3HT exciton states.

At short pump-probe time delays, both positive sand negative pump-probe signals are dominated by ultrafast decays with subpicosecond time constants for the pristine polymer and the P3HT:PCBM sample and slightly longer time constants for the QD-containing samples. Similar to our early interpretations the fast decays are attributed to hot exciton relaxation effects. The signal rise of non-QD containing films is fast, limited by the laser pulse width while QD-containing samples exhibit visibly slower rise times (see Figs. 8 and 9 (a) and (c)). This is in general agreement with transient experiments in processed devices[12] in which hybrid QD devices were found to have a slower transient response compared to all-organic photodiodes. The slow rise of the signal indicates the presence of an energy state that originates in the QDs and replenishes the P3HT exciton states with charge excitations in a time-scale of the order of 1 ps. Electronic relaxation of high energy core and/or surface QD states[17] populated at energies high above the energy gap of PbS QDs, such as the situation encountered in our experiments, could occur at the timescales of the effect observed so that such states could potential be the origins of the transferred excitations. At longer pump-probe delays (5-500 ps) the dynamics in the ternary samples exhibit a behavior variety, with a negligible decay at a probe of 500 nm (Figure 9d), rise of the photobleaching at a probe of 550 nm (Figure 9e), (f)) and relatively long-lived decays of both photoinduced absorption and bleaching at a probe of 600 nm (Figure 9f). The long-lived growth of the photobleaching signal at the probe of 550 nm, observed in all the ternary samples apart from that of the lower QD content, is solely observed in QD-blends and it appears to scale with QD content being especially visible at the highest QD content blend (80%). The effect is attributed to a process that feeds the P3HT exciton states with trapped long-lived excitations. Such excitations may be trapped states within the polymer formed by structural modifications on the polymer packing due to the incorporation of a high QD content; this is consistent with the observed smoothing on the polymer absorption structure with high QD content. Alternatively excitations in long-lived trapped states of the PbS NCs could be also responsible. At the third probe wavelength of 600 nm, photobleaching is visible only in the lowest QD content sample that exhibits a long decay of the bleaching signal with a lifetime comparable to values reported for P3HT fluorescent excitons.

3. Conclusions

We have performed a systematic study of the optical properties of pristine samples and binary and ternary blends based on conjugated polymers (P3HT), fullerenes (PCBM) and colloidal nanocrystals (oleic-capped PbS QDs) using a combination of steady-state and time-resolved optical techniques. The samples studied share identical characteristics to the active region of recently reported high performance near-infrared organic photodetectors.[12] Steady-state absorption shows a modest increase of the red and near-infrared light harvesting efficiency upon addition of the QDs. Photoluminescence experiments performed in the spectral regions of the P3HT and the QDs emission, show partial quenching of the blends PL in respect to the emission of the pristine films. Emission quenching in the polymer region is attributed to re-absorption by the QDs and to electron transfer predominantly to PCBM and to a lesser degree to the nanocrystals. On the other hand QD emission is predominantly quenched due to electron transfer to PCBM and/or hole transfer to P3HT. Ultrafast transient absorption measurements reveal a variety of relaxation pathways of P3HT photogenerated species in the blends. At short times, relaxation in all samples is dominated by linear hot exciton relaxation effects. At longer times, long-lived components attributed to charge-transfer excitons are observed. The formation of such species occurs efficiently at samples with large content of P3HT and PCBM components while it is found to be quenched at the binary P3HT:QDs sample and the pristine P3HT film. At short probe wavelengths, coincident with the ground states of the P3HT singlet exciton, a long-lived photobleaching of the state is observed at QD-containing blends. Overall both steady-state PL experiments and transient absorption measurements indicate that interfacial charge transfer processes occur more efficiently at the fullerene/polymer and fullerene/nanocrystal interfaces compared to polymer/nanocrystal interfaces. Thus the inclusion of the fullerene seems to facilitate exciton dissociation in such ternary blends. Further work to investigate the contribution of (i) surface/trap QD states[17], (ii) dielectric effects[35], (iii) intermaterial band alignment and morphology[12,29] and (iv) QD organic ligand role[36] and exchange[37] could provide answers on why PbS QDs perform well in all-QD Schottky solar cells i.e.[38] while being rather inefficient in QD-sensitized organic photovoltaics.

4. Experimental Section

Sample preparation: Oleic acid capped PbS nanocrystals were synthesized following the procedure of reference 39. All studied samples contain QDs with a nominal diameter size of 4.4 nm and a diameter size dispersion of 10–15%. RR-P3HT was purchased from Rieke Metals and C60-PCBM from Solenne. All materials were dissolved in chlorobenzene at ~2 wt.%, under nitrogen atmosphere in a glovebox. Subsequently to film deposition to glass substrates via doctor-blading an annealing process at 80 °C for 30 min under inert atmosphere was carried out.

Absorption: Measurements on the films were performed in the 250-1500 nm range with a spectral resolution of 0.5 nm using a UV-VIS-nearIR spectrophotometer.

Photoluminescence: PL experiments were carried out using a 0.75m spectrometer equipped with a CCD camera and an InGaAs array detector to record the spectra in the spectral region of the polymer and nanocrystal emission, respectively. All PL data have been acquired with samples in vacuum conditions (~10^{-3} mbar). The P3HT fluorescence was excited with a 405 nm diode laser to predominantly photoexcite the polymer component of the blends i.e. at 405 nm the absorption of P3HT is significantly higher compared to the two other material components. Similarly a 785 nm diode laser was employed for the measurements of the nanocrystal luminescence to selectively photoexcite only the QD component of the blends. The PL measurements were performed on a side by side geometry to allow a direct emission-intensity comparison. To correct for sample spatial variations due to thickness and concentration fluctuations a number of different spots were probed across the samples surfaces. The quenching ratios were obtained by measuring the average of the integrated emission from all the spots probed while the standard deviation of the measurements was defined as its error. Excitation dependent PL measurements were performed in the 0.1-6.5 W/cm^2 region.

Pump-probe: Samples were excited at inert nitrogen atmosphere using a self mode-locked Ti:Sapphire oscillator generating 100 fs pulses at 800 nm. A chirped pulsed laser amplifier based on a regenerative cavity configuration was used to amplify the pulses to approximately 1 mJ at a repetition rate of 1 kHz. Part of the energy was used was used to frequency double the fundamental to 400 nm using a non-linear BBO crystal. A small fraction of the fundamental energy was also used to generate a super continuum white light by focusing the beam on a sapphire plate. The white light probe beam was used in a non-collinear geometry, in a pump-probe configuration where the pump beam was generated from the frequency doubling of the fundamental. The reflected and transmission beams were separately directed onto their respective silicon detectors after passing through a bandpass filter selecting the probe wavelength from the white light.

Acknowledgements

G. Itskos thanks the University of Cyprus for financial support via start-up funds and Cyprus Research Promotion Foundation for financial support via the infrastructure upgrade research grant "ANABAΘMIΣH/0609/15". S. A. Choulis thanks Cyprus University of Technology for the OPV based starting research grant and Cyprus Research Promotion Foundation for funding the development of the Molecular Electronics and Photonics Research Unit under research grant "NEA ΥΠΟΔΟΜΗ/ΣΤΡΑΤΗ/0308/06". W. Heiss and M. V. Kovalenko thank the Austrian Science Fund FWF for financial support via the SFB Project IR_ON. We thank V. Klüppel, T. Ohnemus and A. Rucki for experimental TEM work included in the manuscript.

Received: April 5, 2011
Revised: May 27, 2011
Published online:

[1] S. H. Park, A. Roy, S. Beaupré, S. Cho, N. Coates, J. S. Moon, D. Moses, D. M. Leclerc, K. Lee, A. J. Heeger, *Nat. Photonics* **2009**, *3*, 297.
[2] Y. Liang, Z. Xu, J. Xia, S. Tsai, Y. Wu, G. Li, C. Ray, L. Yu, *Adv. Mater,*. **2010**, *22*, E135.
[3] J. A. Hauc, P. Schilinsky, S. A. Choulis, R. Childers, M. Biele, C. J. Brabec, *Sol. Energy Mater. Sol. Cells* **2008**, *92*, 727.
[4] C. N. Hoth, P. Schilinsky, S. A. Choulis, C. J. Brabec, *Nano Lett.*, **2008**, *8*, 2806.
[5] F. C. Krebs, *Sol. Energy Mater. Sol. Cells* **2009**, *93*, 394.
[6] E. Bundgaard, F. C. Krebs, *Sol. Energy Mater. Sol. Cells* **2007**, *91*, 954.
[7] C. J. Brabec, J. R. Durrant, *MRS Bullet.* **2008**, *33*, 670.
[8] N. C. Greenham, X. Peng, A. P. Alivisatos, *Phys. Rev. B* **1996**, *54*, 17628.
[9] E. H. Sargent, *Nat. Photonics* **2009**, *3*, 325.
[10] E. H. Sargent, *Adv. Mater.* **2008**, *20*, 3958.
[11] G. Konstantatos, E. H. Sargent, *Nat. Nanotechnology* **2010**, *5*, 391.
[12] T. Rauch, M. Böberl, S. F. Tedde, J. Fürst, M. V. Kovalenko, G. Hesser, U. Lemmer, W. Heiss, O. Hayden, *Nat. Photonics* **2009**, *3*, 332.
[13] K. M. Noone, E. Strein, N. C. Anderson, P.-T. Wu, S. A. Jenekhe, D. S. Ginger, *Nano Lett.* **2010**, *10*, 2635.
[14] B. Sun, A. T. Findikoglu, M. Sykora, D. J. Werder, V. I. Klimov, *Nano Lett.* **2009**, *9*, 1235.
[15] J. M. Luther, M. Law, M. C. Beard, Q. Song, M. O. Rees, R. J. Ellingson, A. J. Nozik, *Nano Lett.* **2008**, *8*, 3488.
[16] N. Zhao, T. P. Osedach, L.-Y. Chang, S. M. Geyer, D. Wanger, M. T. Binda, A. C. Arango, M. G. Bawendi, V. Bulovic, *ACS Nano* **2010**, *4*, 3743.
[17] A. L. Rogach, A. Eychmüller, S. G. Hickey, S. V. Kershaw, *Small* **2007**, *3*, 536.
[18] V. Shrotriya, J. Ouyang, R. J. Tseng, G. Li, Y. Yang, *Chem. Phys. Lett.* **2005**, *411*, 138.
[19] K. Pichler, S. Graham, O. M. Gelsen, R. H. Friend, W. J. Romanow, J. P. McCauley Jr, N. Coustel, J. E. Fischer, A. B. Smith, *J. Phys: Cond. Matt.*, **1991**, *3*, 9259.
[20] D. Chirvase, J. Parisi, J. C. Hummelen, V. D. Dyakonov, *Nanotechnology* **2004**, *15*, 1317.
[21] A. C. Mayer, M. F. Toney, S. R. Scully, J. Rivnay, C. J. Brabec, M. Scharber, M. Koppe, M. Heeney, I. McCulloch, M. D. McGehee, *Adv. Funct. Mater.* **2009**, *19*, 1173.
[22] X. Ai, M. C. Beard, K. P. Knutsen, S. E. Shaheen, G. Rumbles, R. J. Ellingson, *J. Phys. Chem. B* **2006**, *110*, 25462.
[23] J. Piris, T. E. Dykstra, A. A. Bakulin, P. H. M. van Loosdrecht, W. Knulst, M. T. Trinh, J. M. Schins, L. D. A. Siebbeles, *J. Phys. Chem. C* **2009**, *113*, 14500.
[24] J. H. Warner, A. R. Watt, E. Thomsen, N. Heckenberg, P. Meredith, H. Rubinsztein-Dunlop, *J. Phys. Chem. B* **2005**, *109*, 9001.
[25] J. H. Warner, A. R. Watt, R. D. Tilley, *Nanotechnology* **2005**, *16*, 2381.
[26] K. Szendrei, F. Cordella, M. V. Kovalenko, M. Böberl, G. Hesser, M. Yarema, D. Jarzab, O. V. Mikhnenko, A. Gocalinska, M. Saba, F. Quochi, A. Mura, G. Bongiovanni, P. W. M. Blom, W. Heiss, M. A. Loi, *Adv. Mater.* **2009**, *21*, 683.
[27] M. D. Heinemann, K. von Maydell, F. Zutz, J. Kolny-Olesiak, H. Borchert, I. Riedel, J. Parisi, *Adv. Funct. Mater.* **2009**, *19*, 3788.
[28] E. Istrate, S. Hoogland, V. Sukhovatkin, L. Levina, S. Myrskog, P. W. E. Smith, E. H. Sargent, *J. Phys. Chem. B Lett.* **2009**, *112*, 2757.
[29] A. Gocalinska, M. Saba, F. Quochi, M. Marceddu, K. Szendrei, J. Gao, M. A. Loi, M. Yarema, R. Seyrkammer, W. Heiss, A. Mura, G. Bongiovanni, *J. Phys. Chem. Lett.* **2010**, *1*, 1149.
[30] I. W. Hwang, D. Moses, A. J. Heeger, *J. Phys. Chem. C* **2008**, *112*, 4350.
[31] P. D. Cunningham, L. M. Hayden, *J. Phys. Chem. C* **2008**, *112*, 7928.
[32] S. Cook, R. Katoh, A. Furube, *J. Phys. Chem. C* **2009**, *113*, 2547.
[33] C. Deibel, T. Strobel, V. Dyakonov, *Adv. Mater.* **2010**, *22*, 4097.
[34] P. Parkinson, J. Lloyd-Hughes, M. B. Johnston, L. M. Hertz, *Phys. Rev. B* **2008**, *78*, 115321-1-11.
[35] T. Takagahara, *Phys. Rev. B* **1993**, *47*, 4569.
[36] P. Podsiadlo, G. Krylova, B. Lee, K. Critchley, D. J. Gosztola, D. V. Talapin, P. D. Ashby, E. V. Shevchenko, *J. Am. Chem. Soc.* **2010**, *132*, 8953.
[37] Y. Wu, G. Zhang, *Nano Lett.* **2010**, *10*, 1628.
[38] K. Szendrei, W. Gomulya, M. Yarema, W. Heiss, M. A. Loi, *Appl. Phys. Lett.* **2010**, *97*, 203501-1.
[39] M. A. Hines, G. D. Scholes, *Adv. Mater.* **2003**, *15*, 1844.